Article

Ab Initio Nonadiabatic Molecular Dynamics of the Ultrafast Electron Injection across the Alizarin–TiO Interface

Walter R. Duncan, William M. Stier, and Oleg V. Prezhdo

J. Am. Chem. Soc., **2005**, 127 (21), 7941-7951• DOI: 10.1021/ja042156v • Publication Date (Web): 04 May 2005

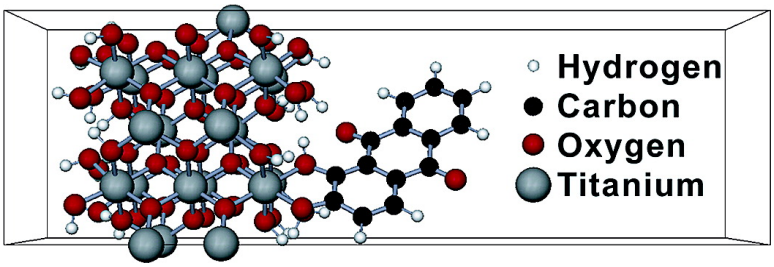

More About This Article

Additional resources and features associated with this article are available within the HTML version:

- Supporting Information
- Links to the 21 articles that cite this article, as of the time of this article download
- Access to high resolution figures
- Links to articles and content related to this article
- Copyright permission to reproduce figures and/or text from this article

View the Full Text HTML

J|A|C|S
ARTICLES
Published on Web 05/04/2005

Ab Initio Nonadiabatic Molecular Dynamics of the Ultrafast Electron Injection across the Alizarin−TiO_2 Interface

Walter R. Duncan, William M. Stier, and Oleg V. Prezhdo*

Contribution from the Department of Chemistry, University of Washington, Seattle, Washington 98195-1700

Received December 30, 2004; E-mail: prezhdo@u.washington.edu

Abstract: The observed 6-fs photoinduced electron transfer (ET) from the alizarin chromophore into the TiO_2 surface is investigated by ab initio nonadiabatic (NA) molecular dynamics in real time and at the atomistic level of detail. The system derives from the dye-sensitized semiconductor Grätzel cell and addresses the problems of an organic/inorganic interface that are commonly encountered in photovoltaics, photochemistry, and molecular electronics. In contrast to the typical Grätzel cell systems, where molecular donors are in resonance with a high density of semiconductor acceptor states, TiO_2 sensitized with alizarin presents a novel case in which the molecular photoexcited state is at the edge of the conduction band (CB). The high level ab initio analysis of the optical absorption spectrum supports this observation. Thermal fluctuations of atomic coordinates are particularly important both in generating a nonuniform distribution of photoexcited states and in driving the ET process. The NA simulation resolves the controversy regarding the origin of the ultrafast ET by showing that although ultrafast transfer is possible with the NA mechanism, it proceeds mostly adiabatically in the alizarin−TiO_2 system. The simulation indicates that the electron is injected into a localized surface state within 8 fs and spreads into the bulk on a 100-fs or longer time scale. The molecular architecture seen in the alizarin−TiO_2 system permits efficient electron injection into the edge of the CB by an adiabatic mechanism without the energy loss associated with injection high into the CB by a NA process.

Introduction

Electron transfer (ET) at organic/inorganic interfaces plays a key role in many areas of research. Intense scientific interest has been devoted to the characterization and understanding of the nature and mechanisms of the interfacial ET.[1−40] In the burgeoning field of molecular electronics, the movement of charge through molecules and solid-state structures has been well described, but transfer across the contacts is still poorly understood and remains the main area of study.[1−6,13−15] The interfacial charge transfer is also the key step in many photoinduced chemical reactions, including reactions that play a central role in photoelectrolysis,[41] photocatalysis,[7−11] and color

(1) Nitzan, A.; Ratner, M. A. *Science* **2003**, *300*, 1384.
(2) Holman, M. W.; Liu, R.; Adams, D. M. *J. Am. Chem. Soc.* **2003**, *125*, 12649.
(3) Fan, F. F.; Yang, J. P.; Cai, L.; Price, D. W.; Dirk, S. M.; Kosynkin, D. V.; Yao, Y. X.; Rawlett, A. M.; Tour, J. M.; Bard, A. J. *J. Am. Chem. Soc.* **2002**, *124*, 5550.
(4) Klare, J. E.; Tulevski, G. S.; Sugo, K.; de Picciotto, A.; White, K. A.; Nuckolls, C. *J. Am. Chem. Soc.* **2003**, *20*, 6030.
(5) Fan, F. F.; Yao, Y.; Cai, L.; Cheng, L.; Tour, J. M.; Bard, A. J. *J. Am. Chem. Soc.* **2004**, *126*, 4035.
(6) Yasutomi, S.; Morita, T.; Imanishi, Y.; Kimura, S. *Science* **2004**, *304*, 1944.
(7) Zhao, W.; Ma, W. H.; Chen, C. C.; Zhao, J. C.; Shuai, Z. G. *J. Am. Chem. Soc.* **2004**, *126*, 4782.
(8) Hirakawa, T.; Whitesell, J. K.; Fox, M. A. *J. Phys. Chem. B* **2004**, *108*, 10213.
(9) Cozzoli, P. D.; Fanizza, E.; Comparelli, R.; Curri, M. L.; Agostiana, A.; Laub, D. *J. Phys. Chem. B* **2004**, *108*, 9623.
(10) Ho, W.; Yu, J. C.; Lin, J.; Yu, J.; Li, P. *Langmuir* **2004**, *20*, 5865.
(11) Kim, H. G.; Hwang, D. W.; Lee, J. S. *J. Am. Chem. Soc.* **2004**, *126*, 8912.
(12) Liu, D.; Hug, G. L.; Kamat, P. V. *J. Phys. Chem.* **1995**, *99*, 16768.
(13) Nitzan, A. *Annu. Rev. Phys. Chem.* **2001**, *52*, 681.
(14) Zhu, X. Y. *J. Phys. Chem. B* **2004**, *108*, 8778.
(15) Derosa, P. A.; Seminario, J. M. *J. Phys. Chem. B* **2001**, *105*, 471.
(16) Oregan, B.; Grätzel, M. *Nature* **1991**, *353*, 737.
(17) Tachibana, Y.; Moser, J. E.; Grätzel, M.; Klug, D. R.; Durrant, J. R. *J. Phys. Chem. B* **1996**, *100*, 20056.
(18) Willig, F.; Zimmermann, C.; Ramakrishna, S.; Storck, W. *Electrochim. Acta* **2000**, *45*, 4565.
(19) Asbury, J. B.; Hao, E. C.; Wang, Y. Q.; Ghosh, H. N.; Lian, T. Q. *J. Phys. Chem. B* **2001**, *105*, 4545.
(20) Huber, R.; Spoerlein, S.; Moser, J. E.; Grätzel, M.; Wachtveitl, J. *J. Phys. Chem. B* **2000**, *104*, 8995.
(21) Huber, R.; Moser, J. E.; Grätzel, M.; Wachtveitl, J. *J. Phys. Chem. B* **2002**, *106*, 6494.
(22) Anderson, N. A.; Hao, E.; Ai, X.; Hastings, G.; Lian, T. *Physica E (Amsterdam)* **2002**, *14*, 215.
(23) Kelly, C. A.; Meyer, G. J. *Coord. Chem. Rev.* **2001**, *211*, 295.
(24) Ramakrishna, S.; Willig, F. *J. Phys. Chem. B* **2000**, *104*, 68.
(25) Ramakrishna, S.; Willig, F.; May, V.; Knorr, A. *J. Phys. Chem. B* **2003**, *107*, 607.
(26) Wang, L. X.; May, V. *J. Chem. Phys.* **2004**, *121*, 8039.
(27) Thoss, M.; Kondov, I.; Wang, H. *Chem. Phys.* **2004**, *304*, 169.
(28) Rego, L. G. C.; Batista, V. S. *J. Am. Chem. Soc.* **2003**, *125*, 7989.
(29) Stier, W.; Prezhdo, O. V. *J. Phys. Chem. B* **2002**, *106*, 8047.
(30) Stier, W.; Prezhdo, O. V. *J. Mol. Struct. (THEOCHEM)* **2002**, *630*, 33.
(31) Stier, W.; Prezhdo, O. V. *Isr. J. Chem.* **2002**, *42*, 213.
(32) Stier, W.; Duncan, W. R.; Prezhdo, O. V. *Adv. Mater.* **2004**, *16*, 240.
(33) Duncan, W. R.; Prezhdo, O. V. *J. Phys. Chem. B* **2005**, *109*, 365.
(34) Kucur, E.; Reigler, J.; Urban, G. A.; Nann, T. *J. Chem. Phys.* **2004**, *120*, 1500.
(35) Anderson, N. A.; Hao, E. C.; Ai, X.; Hastings, G.; Lian, T. Q. *Chem. Phys. Lett.* **2001**, *347*, 304.
(36) Arango, A. C.; Johnson, L. R.; Bliznyuk, V. N.; Schlesinger, Z.; Carter, S. A.; Horhold, H. H. *Adv. Mater.* **2001**, *12*, 1689.
(37) Greens, W.; Martens, T.; Poortmans, J.; Aernouts, T.; Manca, J.; Lutsen, L.; Heremans, P.; Borghs, S.; Mertens, R.; Vanderzande, D. *Thin Solid Films* **2004**, *451−452*, 498.
(38) Hao, E.; Anderson, N. A.; Asbury, J. B.; Lian, T. *J. Phys. Chem. B* **2002**, *106*, 10191.
(39) Ravirajan, P.; Haque, S. A.; Poplavskyy, D.; Durrant, J. R.; Bradley, D. D. C.; Nelson, J. *Thin Solid Films* **2004**, *451−452*, 624.
(40) Nozik, A. J. *Physica E (Amsterdam)* **2002**, *14*, 115.

photography.[12] ET at semiconductor interfaces constitutes the primary step in many novel photovoltaic devices comprising dye-sensitized semiconductors,[16−25,42,43] assemblies of inorganic semiconductors with conjugated polymers,[34−39] and quantum confinement devices.[40,44] Here too the exact mechanistic details of the interfacial ET are an issue of debate. The current paper reports a detailed real-time ab initio analysis of the observed[21] record ultrafast electron injection from an alizarin molecule into the TiO_2 surface. The system derives from the dye-sensitized semiconductor Grätzel cell and is an excellent model for processes that occur in many of the above fields of application. The presented analysis uncovers a number of novel features of the injection process that are not observed in the previously studied cases,[24−33,45−52] and have important fundamental and practical implications.

The alizarin−TiO_2 interface is a particular example of the photoinduced charge separation component in the Grätzel cell, where highly porous nanocrystalline titanium dioxide is sensitized with transition metal or organic dye molecules.[54,16] Grätzel cells offer a promising alternative to the more costly traditional solar cells.[16] When they absorb light, the dye-sensitizer molecules are excited from their ground state, which is located energetically in the semiconductor band gap, to an excited state that is resonant with the TiO_2 conduction band (CB) (Figure 1). The electron is then transferred on the ultrafast time scale to the semiconductor, which is in contact with one of the electrodes. Upon carrying an electric load and reaching the second electrode, the electron enters an electrolyte that carries it back to the chromophore ground state. The relative yields and rates of electron injection, recombination, and decay of the photoexcited-state all influence the efficiency of the solar cell.[55,56] Large photocurrents require dyes with high extinction coefficients, slow electron−hole recombination, and fast ET. Large voltages result from small losses due to relaxation of the electron across the chromophore vibronic manifold and, after the injection, inside the semiconductor CB. Grätzel cells generally show a high photon-to-electron energy conversion yield; low photovoltage, however, remains a limiting factor.[56] Improving the efficiency of the solar devices is possible only when the rates and mechanisms of the competing reactions are known and understood.

Numerous experimental groups have investigated ET dynamics in Grätzel cells.[17−23] The injection rate has been found to depend on the electronic properties of both the dye and the semiconductor, as well as the distance between the two, as determined by the length of the molecular bridge. Lian and coworkers[19] found that ET between ruthenium-based dyes and TiO_2 occurred on a femtosecond time scale, whereas ET between the same dyes attached to SnO_2 and ZnO were orders of magnitude slower. A similar effect was observed after the length of the bridging units between the dye and the semiconductor were changed: increasing the dye−semiconductor distance dramatically slowed the ET. By altering the redox potential of the dyes attached to SnO_2, Lian et al. were able to affect a range of electron-transfer times, while the same dyes attached to TiO_2 all had electron injection times of less than 100 fs.[19] These and other experimental data clearly point to a complex dependence of the ET rates and mechanisms on the chemical and electronic structure of the organic dyes, the inorganic semiconductor, and the dye−semiconductor binding.

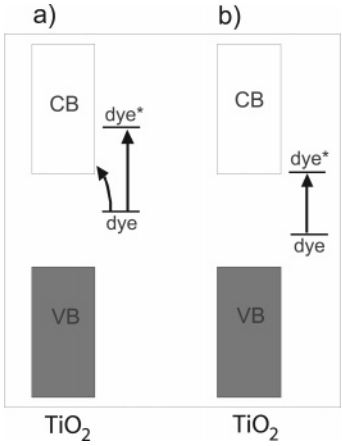

Figure 1. Photon absorption promotes an electron from the ground state of the dye located inside the semiconductor energy gap into an excited state that is in resonance with the conduction band (CB). (a) The dye excited state is well inside the CB, and an additional direct photoexcitation from the dye ground state into a semiconductor state near the CB edge becomes possible with a strong coupling as in the catechol−TiO_2 system.[22,28,33,53] (b) The dye excited state is near the edge of the TiO_2 CB as in the alizarin−TiO_2 system considered here.

Ultrafast laser techniques have shown that electron injection can occur in less than 100 fs,[18−21] making it difficult to invoke traditional ET models, which require slow ET dynamics to allow for redistribution of vibrational energy.[18,58] Two competing ET mechanisms have been proposed to explain the observed ultrafast injection events.[19,59] These mechanisms have drastically different implications for the variation of the interface conductance and solar cell voltage with system properties. In the adiabatic mechanism, the coupling between the dye and the semiconductor is large, and ET occurs through a transition state (TS) along the reaction coordinate that involves a concerted motion of nuclei (Figure 2). During adiabatic transfer, the electron remains in the same Born−Oppenheimer (adiabatic) state that continuously changes its localization from the dye to the semiconductor along the reaction coordinate. The adiabatic mechanism is a typical chemical phenomenon and forms the basis of TS theories, in which the reaction rate is determined by the probability of finding and crossing the TS.[57] A small TS

(41) Jiang, D. L.; Zhao, H. J.; Zhang, S. Q.; John, R. *J. Catal.* **2004**, *223*, 212.
(42) Pan, J.; Benko, G.; Xu, Y. H.; Pascher, T.; Sun, L. C.; Sundstrom, V.; Polivka, T. *J. Am. Chem. Soc.* **2002**, *124*, 13949.
(43) Biju, V.; Micic, M.; Hu, D. H.; Lu, H. P. *J. Am. Chem. Soc.* **2004**, *126*, 9374.
(44) Schaller, R. D.; Klimov, V. I. *Phys. Rev. Lett.* **2004**, *92*, 186601.
(45) Nazeeruddin, M. K.; Zakeeruddin, S. M.; Humphry-Baker, R.; Gorelsky, S. I.; Lever, A. B. P.; Grätzel, M. *Coord. Chem. Rev.* **2000**, *208*, 213.
(46) Srikanth, K.; Marathe, V. R.; Mishra, M. K. *Int. J. Quant. Chem.* **2002**, *89*, 534.
(47) Aiga, F.; Tada, T. *J. Mol. Struct.* **2003**, *658*, 25.
(48) Persson, P.; Lunell, S.; Ojamäe, L. *Chem. Phys. Lett.* **2002**, *364*, 469.
(49) Odelius, M.; Persson, P.; Lunell, S. *Surf. Sci.* **2003**, *529*, 47.
(50) Persson, P.; Bergström, R.; Lunell, S. *J. Phys. Chem. B* **2000**, *104*, 10348.
(51) Rego, L. G. C.; Abuabara, S. G.; Batista, V. S. *J. Chem. Phys.* In press.
(52) Rego, L. G. C.; Abuabara, S. G.; Batista, V. S. *Quantum Inform. Comput.* In press.
(53) Wang, Y.; Hang, K.; Anderson, N. A.; Lian, T. *J. Phys. Chem. B* **2003**, *107*, 9434.
(54) Schwarz, O.; van Loyen, D.; Jockusch, S.; Turro, N. J.; Duerr, H. *J. Photochem. Photobiol. A: Chem.* **2000**, *132*, 91.
(55) McConnell, R. D. *Renew. Sustain. Energy Rev.* **2002**, *6*, 273.
(56) Huang, S. Y.; Schlichthorl, G.; Nozik, A. J.; Gratzel, M.; Frank, A. J.; *J. Phys. Chem. B* **1997**, *101*, 2576.
(57) Memming, R. *Semiconductor Electrochemistry*; Wiley-VCH: Weinheim, 2001.
(58) Hannappel, T.; Burfeindt, B.; Storck, W.; Willig, F. *J. Phys. Chem. B* **1997**, *101*, 6799.
(59) Asbury, J. B.; Ellingson, R. J.; Ghosh, H. N.; Nozik, A. J.; Ferrere, S.; Lian, T. *J. Phys. Chem. B* **1999**, *103*, 3110.

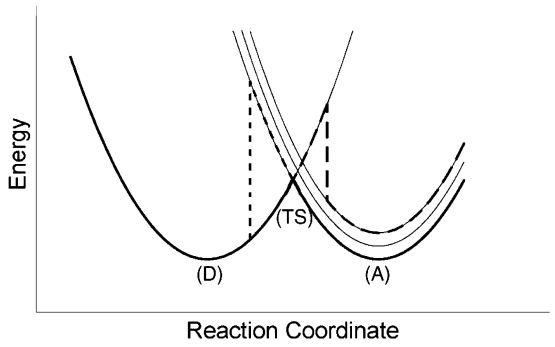

Figure 2. Adiabatic and nonadiabatic (NA) pathways of electron transfer (ET). As in the Marcus theory,[57] the parabolas describe the donor state (D) localized on alizarin and a set of acceptor states (A) localized on TiO_2. The bold solid line represents adiabatic ET from D and A through a transition state (TS). NA ET involves direct quantum transitions between D and A (dashed lines) that can occur regardless of the TS.

barrier relative to the nuclear kinetic energy gives fast adiabatic ET. Nonadiabatic effects (NA) decrease the amount of ET that happens at the TS but open up a new channel involving direct transitions from the dye into the semiconductor that can occur at any nuclear configuration. NA transfer becomes important when the dye−semiconductor coupling is weak and is often described by perturbation theory, as in the case of Fermi's golden rule,[57] where the rate of transfer is proportional to the density of acceptor states. NA ET is a quantum effect and, similar to tunneling, shows exponential dependence on the donor−acceptor separation.

Theoretical studies of the dye-sensitized semiconductor systems have focused on chromophore−semiconductor binding,[60−63] electronic structure and spectra of free and bound chromophores,[45−50] as well as direct simulation of the electron injection dynamics.[24−32] Investigations into the dye−semiconductor binding have been conducted for a number of different systems, including formic acid and sodium formate on the stoichiometric anatase TiO_2 (101) surface,[62] formic acid on the ZnO $(10\bar{1}0)$ surface,[61] bi-isonicotinic acid on anatase TiO_2 (101),[63] and catechol on TiO_2 nanoparticles.[60] The electronic structure and spectra of the dye−semiconductor systems have been the subject of a number of theoretical studies,[45−50] focusing both on ruthenium-based dyes[45−47] and organic dye systems.[50,33] The Grätzel group[45] performed geometry optimizations of *cis*- and *trans*-(Cl_2)bis(4,4′-dicarboxylic acid-2,2′-bipyridine)ruthenium(II) complexes with DFT and then calculated the electronic spectra by ZINDO/S. They found that the three highest occupied molecular orbitals (HOMO) were formed mostly from the 4d orbitals of Ru, while the lowest unoccupied molecular orbitals (LUMO) were almost entirely localized on two $dcbpyH_2$ ligands. The intense absorption in the visible region was assigned to the HOMO−LUMO transition. Lunell and co-workers[50] performed quantum chemical INDO/S-CI calculations of anatase TiO_2 nanoparticles that had been sensitized by catechol and benzoic acid. The experimental observation that catechol causes a strong shift in the TiO_2 absorption threshold, whereas benzoic acid does not, was explained by the calculation that indicated that only catechol introduces electronic levels into the TiO_2 band gap.

Direct modeling of the ultrafast electron injection processes between dyes and semiconductors observed in laser experiments[17−22] has been performed with reduced models and a full quantum-mechanical description of electrons and nuclei[24−27] or at a detailed atomistic level using a quantum description of electrons and classical treatment of nuclei.[28−32,51,52] To interpret their pump−probe experimental data and explain the observed coherent oscillations in the spectroscopic signal, Willig and co-workers[24−26] developed a few-dimensional quantum model of the ultrafast electron injection in perylene-sensitized TiO_2. Thoss and co-workers[27] adopted a generic model for the heterogeneous ET to study the influence of coherent and dissipative vibrational motion on the ET dynamics. The first real-time atomistic simulations of the interfacial ET from isonicotinic acid into TiO_2 were carried out in our group[30,31] using ab initio nonadiabatic molecular dynamics. Batista and co-workers[28,51,52] used quantum dynamics calculations of electronic relaxation to study ET in the catechol/TiO_2-anatase system. Both methods reproduced the experimental ultrafast electron injection. Having used the semiempirical Hückel Hamiltonian for electron relaxation dynamics in combination with an ab initio description of atomic configurations, Batista and co-workers were able to simulate a larger system and follow anisotropic charge diffusion through the TiO_2 crystal. By treating coupled electron−nuclear dynamics, we were able to describe both adiabatic and nonadiabatic ET mechanisms. Our ab initio simulations of the coupled electron−nuclear dynamics established the electron injection mechanism that varied at low and high temperatures and identified the nuclear motions promoting the ET.[30,31]

Many researchers have assumed that a high density of semiconductor states is needed for fast and efficient ET. The dye is typically chosen to have an excited state well within the semiconductor CB (Figure 1a).[16−19,36,55,56,64−66] The simulations of the electron injection dynamics have therefore been performed for systems with chromophore excited states substantially above the band edge. The alizarin/TiO_2 system represents an interesting and novel case in which the photoexcited state is positioned near the band edge. This is evidenced both by the experimental data[20,21] and quantum-chemical calculations.[33] Experiments show that electron injection from the alizarin excited state near the TiO_2 CB edge is no less efficient than ET from chromophores with excited states deep in the CB. On the contrary, the injection is extremely fast with a record 6-fs transfer time.[21] Efficient ultrafast injection from photoexcited states near the CB edge is both fundamentally interesting and practically important. The fundamental question is: what mechanisms make the ET so fast in the absence of a high density of acceptor states? On the practical side, injection at the CB edge has the potential to aid in the design of cells with higher maximum theoretical voltage, since energy will not be lost by rapid relaxation to the bottom of the CB.[67]

In the following section of this paper we present a theoretical analysis of the electronic structure and absorption spectrum of

(60) Redfern, P. C.; Zapol, P.; Curtiss, L. A.; Rajh, T.; Thurnauer, M. C. *J. Phys. Chem. B* **2003**, *107*, 11419.
(61) Persson, P.; Lunell, S.; Ojamäe, L. *Int. J. Quant. Chem.* **2002**, *89*, 172.
(62) Vittadini, A.; Selloni, A.; Rotzinger, F. P.; Grätzel, M. *J. Phys. Chem. B* **2000**, *104*, 1300.
(63) Persson, P.; Lunell, S. *Sol. Energy Mater. Sol. Cells* **2000**, *63*, 139.
(64) O'Regan, B.; Schwartz, D. T.; Zakeeruddin, S. M.; Grätzel, M. *Adv. Mater.* **2000**, *12*, 1263.
(65) Kruger, J.; Bach, U.; Grätzel, M. *Adv. Mater.* **2000**, *12*, 447.
(66) Nogueira, A. F.; Durrant, J. R.; Paoli, M. A. D. *Adv. Mater.* **2001**, *13*, 826.
(67) Grätzel, M. *J Photochem. Photobiol. C: Photochem. Rev.* **2003**, *4*, 145.

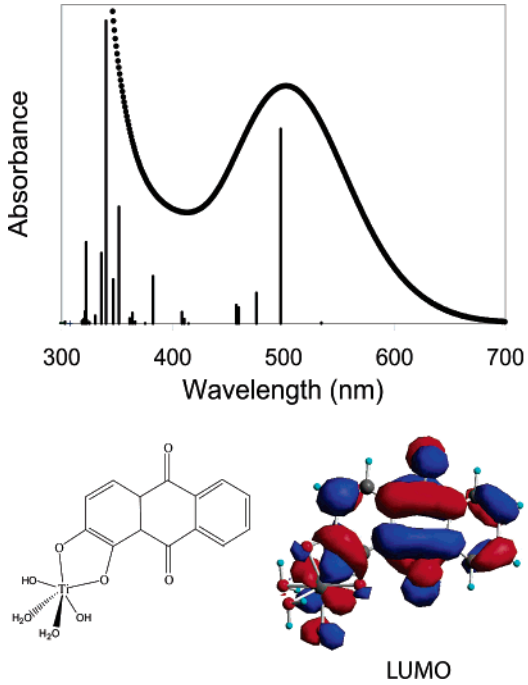

Figure 3. Absorption spectrum of alizarin bound to TiO_2 measured experimentally[20] (merging black dots) and calculated theoretically (lines) with TDDFT. The lower energy band is dominated by a single optically active transition promoting an electron from the HOMO to the LUMO. Bottom frame: chemical structure and LUMO of alizarin bound to a Ti^{4+} ion as expected in solution. The LUMO of the alizarin−TiO_2 system matches the LUMO of free alizarin in agreement with experiments[20] that show little change in the spectrum upon binding.

alizarin attached to TiO_2 and describe the ab initio nonadiabatic molecular dynamics approach to the real-time atomistic simulation of the ET events. The results section then reports details of the molecular donor and surface acceptor states and the role of nuclear dynamics in both generating an inhomogeneous ensemble of initial conditions and promoting ET dynamics. Competition between the adiabatic and NA ET mechanisms is elucidated. We conclude with a summary of the key results.

Theory

Alizarin molecules bind to TiO_2 by the interaction of electron pairs on the hydroxyl oxygens in alizarin with the d-orbitals of Ti atoms. Among the feasible binding motifs (including molecular adsorption, chemical binding through one Ti−O bond, through two Ti−O bonds directed at a single or two separate Ti atoms, as well as a number of possibilities involving tautomerism and hydrogen migration in alizarin) the most stable geometry corresponds to the bidentate structure with two chemical bonds directed to the same surface titanium. This conclusion follows from the ab initio molecular orbital and DFT studies by Thurnauer's group[60] on the related catechol molecule. The tautomeric structures available with alizarin are not possible with catechol; however, the tautomerism destabilizes the molecular π-system and requires additional energy. The present study uses the bidentate binding (Figures 3 and 4).

Electronic Structure and Spectrum. The excitation spectra of the alizarin molecule, both in its free state and when bound to titanium, are similar in shape.[20] The lowest energy band in the electronic spectrum of alizarin bound to TiO_2 is centered around 500 nm (Figure 3) and is red-shifted relative to free alizarin by about 70 nm. The next band is much stronger and occurs below 400 nm. The experimentally observed 6-fs electron injection process takes place after the system is excited at the wavelength of the lowest energy band.[21] The electronic origin of this excitation is elucidated below.

The electronic structure calculations of the absorption spectrum are performed with density functional theory (DFT), which includes electron correlation effects and shows good agreement with the experimental data. A pure DFT PW91 functional due to Perdew and Wang[68] is used. The functional depends on the local one-electron density and its gradient and has been implemented for both finite systems in Gaussian bases[69] and for infinite periodic systems using plane waves.[70−72] Functionals that include contributions from the exact Hartree−Fock exchange term, such as the widely popular B3LYP functional, are not easily implemented for periodic systems and, for this reason, are not used here. A high-level finite system calculation is performed using linear-response time-dependent (TD) DFT in order to establish the electronic structure of the photoexcited state. The calculation is performed with the Gaussian 98 software package using the 6-31g** basis.[69] The electron injection dynamics are investigated with NA TDDFT using the VASP code, the same PW91 functional, periodic boundary conditions, and a plane wave basis.[70−72] By using a converged plane wave basis we avoid the questions associated with the choice of a Gaussian basis, where diffuse functions may be necessary for describing excited states.[73]

The absorption spectrum of alizarin bound to TiO_2 is simulated by performing an electronic structure calculation on a system representing the binding of alizarin to the Ti^{4+} ion in solution (Figure 3). There is excellent agreement with the experimental spectrum.[20] Although it is known that TDDFT can significantly underestimate the energies of long-range charge transfer (CT) states,[74−76] that is not the case with the present calculation, in which the photoexcited state shows moderate and relatively short-ranged CT. Further calculations with the extended periodic system confirm that the influence of TiO_2 on the electronic excitation spectrum of alizarin is well represented by Ti^{4+} with water and hydroxyl ligands. The experimentally observed similarity of the spectra of the closely related catechol molecule bound to bulk TiO_2 and to Ti^{4+} in solution[53] also supports this conclusion.

The experimental and theoretical electronic excitation spectra of alizarin bound to TiO_2 are represented in Figure 3 by black dots merging into a thick black line and a set of vertical lines, respectively. The calculation shows that the lowest energy band

(68) Perdew, J. P.; Burke, K.; Wang, Y. *Phys. Rev. B* **1996**, *54*, 16533.
(69) Frisch, M. J.; Trucks, G. W.; Schlegel, H. B.; Scuseria, G. E.; Robb, M. A.; Cheeseman, J. R.; Zakrzewski, V. G., Jr.; Montgomery, J. A.; Stratmann, R. E.; Burant, J. C.; Dapprich, S.; Millam, J. M.; Daniels, A. D.; Kudin, K. N.; Strain, M. C.; Farkas, O.; Tomasi, J.; Barone, V.; Cossi, M.; Cammi, R.; Mennucci, B.; Pomelli, C.; Adamo, C.; Clifford, S.; Ochterski, J.; Petersson, G. A.; Ayala, P. Y.; Cui, Q.; Morokuma, K.; Malick, D. K.; Rabuck, A. D.; Raghavachari, K.; Foresman, J. B.; Cioslowski, J.; Ortiz, J. V.; Stefanov, B. B.; Liu, G.; Liashenko, A.; Piskorz, P.; Komaromi, I.; Gomperts, R.; Martin, R. L.; Fox, D. J.; Keith, T.; Al-Laham, M. A.; Peng, C. Y.; Nanayakkara, A.; Gonzalez, C.; Challacombe, M.; Gill, P. M. W.; Johnson, B.; Chen, W.; Wong, M. W.; Andres, J. L.; Gonzalez, C.; Head-Gordon, M.; Replogle, E. S.; Pople, J. A. *Gaussian 98*; Gaussian, Inc.: Pittsburgh, PA, 1998.
(70) Kresse, G.; Hafner, J. *Phys. Rev. B* **1994**, *49*, 14251.
(71) Kresse, G.; Furthmüller, J. *Comput. Mater. Sci.* **1996**, *6*, 15.
(72) Kresse, G.; Furthmüller, J. *Phys. Rev. B* **1996**, *54*, 11169.
(73) Furche, F.; Ahlirch, R. *J. Chem. Phys.* **2002**, *117*, 7433.
(74) Dreuw, A.; Weisman, J. L.; Head-Gordon, M. *J. Chem. Phys.* **2003**, *119*, 2943.
(75) Dreuw, A.; Head-Gordon, M. *J. Am. Chem. Soc.* **2004**, *126*, 4007.
(76) Prezhdo, O. V. *Adv. Mater.* **2002**, *14*, 592.

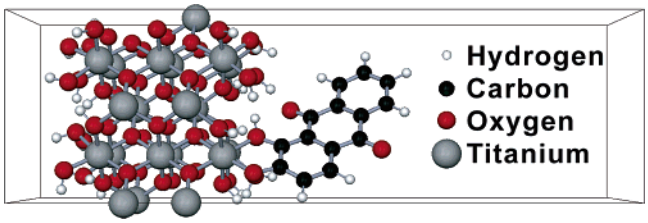

Figure 4. The chromophore−semiconductor simulation cell.

is dominated by a single electronic excitation, with minor contributions from several other less optically active excitations. The broad second band is formed by a large number of excitations. The dominant lowest energy excitation originates by transition of an electron from the highest occupied molecular orbital (HOMO) to the lowest unoccupied molecular orbital (LUMO) of the combined system. The latter is shown under the spectrum and is positioned slightly below the edge of the TiO_2 CB, as follows from the analysis of the experimental[20] and theoretical[33] spectra of free and surface-bound alizarin. Coupling to the CB states slightly lowers the energy of the excited state of the surface-bound alizarin, resulting in a 70 nm redshift. The subsequent electron injection proceeds from this LUMO. The alizarin LUMO is lower in energy than the LUMOs of carbon-based Grätzel cell chromophores due to oxygens, which possess strong electron affinity. Both the HOMO and the LUMO are formed by the π-electrons of the alizarin molecule with a small contribution from the Ti d-orbitals. The HOMO is localized more toward the hydroxyl end of alizarin, while the LUMO is evenly spread over the whole molecule. The HOMO−LUMO photoexcitation redistributes only a small amount of electron density between alizarin and titanium, such that the charge on alizarin remains the same in the ground and excited states.[33]

***Ab Initio* Nonadiabatic Molecular Dynamics.** The experimental pump−probe studies of ET use colloidal particles of TiO_2[20,21] that are prepared by hydrolysis of $TiCl_4$ in cold water[77] and have a high content of anatase, which can spontaneously reconstruct to the more thermodynamically stable rutile structure. Both anatase and rutile particles are characterized by a widespread and unknown distribution of the exposed surfaces and by surface defects that are accessible for the binding of alizarin. While a broad distribution of binding sites and modes may be expected, the large computational expense of the reported study limits the current choice to a single typical binding configuration (Figure 4). In the simulation, the alizarin chromophore is bound to a single titanium atom on the (100) surface of rutile through both hydroxyl groups. The bidentate binding mode has been proposed in the computational studies of the related catechol and water molecules interacting with TiO_2 nanoparticles.[60] Rutile is chosen over anatase, since a mixture of anatase and rutile particles can be converted to pure rutile by heating. The (100) surface of rutile is chosen over the other common (110) surface because the interaction of water with (110) is more complex and to some extent controversial[78,79] and because the (100) surface requires a smaller simulation cell. The system composed of alizarin bound to the rutile (100) surface is simple to reproduce experimentally. It may be expected that the results obtained for the rutile surface will be characteristic of the entire class of interfacial electron injection reactions.

The simulation cell comprises a semiconductor slab five layers thick, with both surfaces terminated by hydroxyl groups and hydrogens, which are attached to the titaniums and the bridging oxygens, respectively.[79] The bottom two layers are frozen in the bulk configuration. Periodic boundary conditions in all three dimensions are used to create an array of TiO_2 slabs. There is a vacuum above and below the TiO_2 surfaces in order to ensure that the slabs in the array do not interact with each other. The dimensions of the cell are $9.3 \times 9.3 \times 30$ Å^3, corresponding to TiO_2 surface coverage of one alizarin molecule per 81 Å^2, or 2 μmol/m^2.

The electronic structure and molecular dynamics (MD) of the combined alizarin/TiO_2 system are computed using density functional theory (DFT) in the plane wave basis, as implemented in the VASP code[70−72] with the NA MD functionality[80−93] added to the standard code distribution.[70−72] Following geometry optimization, the alizarin−TiO_2 structure is brought to equilibrium at ambient temperature by MD with repeated velocity rescaling. A ground-state adiabatic MD simulation is then performed in the microcanonical ensemble with a 1-fs time step. The simulations of the isonicotinic acid−TiO_2 system at ambient temperatures that our group previously performed[31] show that the ET dynamics are dominated by random thermal ionic fluctuations that are similar in the ground and excited states. This is also true of the alizarin−TiO_2 system, where the forces on the ions that result from the electronic excitation are small compared to those that result from random thermal motions. Because the thermal motions dominate, the NAMD calculations can be greatly simplified by using the ground-state trajectory for the description of the ion dynamics during the ET events.

The NA effects in the ET dynamics are described by TDDFT[94,95] within the Kohn−Sham (KS) approach,[96] where the charge density $\rho(\mathbf{r}, t)$ is expressed by a sum over the KS orbitals $\psi_n(\mathbf{r}, t)$ occupied by N_e electrons:

$$\rho(\mathbf{r}, t) = \sum_{n=1}^{N_e} |\psi_n(\mathbf{r}, t)|^2 \qquad (1)$$

The density depends on time through the external potential

(77) Moser, J.; Gratzel, M. *J. Am. Chem. Soc.* **1983**, *105*, 6547.
(78) Shapovalov, V.; Wang, Y.; Truong, T. N. *Chem. Phys. Lett.* **2003**, *375*, 321.
(79) Zhang, Z.; Fenter, P.; Cheng, L.; Sturchio, N. C.; Bedzyk, M. J.; Predota, M.; Bandura, A.; Kubicki, J. D.; Lvov, S. N.; Cummings, P. T.; Chialvo, A. A.; Ridley, M. K.; Benezeth, P.; Anovitz, L.; Palmer, D. A.; Machesky, M. L.; Wesolowski, D. J. *Langmuir* **2004**, *20*, 4954.
(80) Tully, J. C. *J. Chem. Phys.* **1990**, *93*, 1061.
(81) Tully, J. C. World Scientific: Singapore, 1998; p 489.
(82) Volobuev, Y. L.; Hack, M. D.; Topaler, M. S.; Truhlar, D. G. *J. Chem. Phys.* **2000**, *112*, 9716.
(83) Coker, D. F. Kluwer Academic Publishers: Netherlands, 1993; p 315.
(84) Batista, V. S.; Coker, D. F. *J. Chem. Phys.* **1997**, *106*, 7102.
(85) Bittner, E. R.; Rossky, P. J. *J. Chem. Phys.* **1995**, *103*, 8130.
(86) Prezhdo, O. V.; Rossky, P. J. *J. Chem. Phys.* **1997**, *107*, 825.
(87) Prezhdo, O. V.; Rossky, P. J. *J. Chem. Phys.* **1997**, *107*, 5863.
(88) Wang, H.; Song, X. Y.; Chandler, D.; Miller, W. H. *J. Chem. Phys.* **1999**, *110*, 4828.
(89) Ben-Nun, M.; Martinez, T. J. *Adv. Chem. Phys.* **2002**, *121*, 439.
(90) Prezhdo, O. V. *J. Chem. Phys.* **1999**, *111*, 8366.
(91) Prezhdo, O. V.; Brooksby, C. *Phys. Rev. Lett.* **2001**, *86*, 3215.
(92) Brooksby, C.; Prezhdo, O. V. *Chem. Phys. Lett.* **2001**, *346*, 463.
(93) Prezhdo, O. V.; Brooksby, C. *Adv. Top. Theor. Chem. Phys.* **2003**, *12*, 339.
(94) Baer, R.; Gould, R. *J. Phys. Chem. B* **2001**, *114*, 3385.
(95) Frauenhelm, T.; Seifert, G.; Elstner, M.; Niehaus, T.; Kohler, C.; Amkreutz, M.; Sternberg, M.; Hajnal, Z.; DiCarlo, A.; Suhai, S. *J. Phys. Condens. Matter* **2002**, *14*, 3015.
(96) Kohn, W.; Sham, L. J. *Phys. Rev.* **1965**, *140*, 1133.

created by the moving ions. The evolution of the electron density is determined by the TD variational principle, leading to the following set of equations of motion for the KS orbitals:

$$i\hbar\frac{\partial}{\partial t}\psi_n(\mathbf{r}, t) = H(\mathbf{r},\mathbf{R}, t)\psi_n(\mathbf{r}, t); \quad n = 1, 2, ..., N_e \quad (2)$$

These one-electron equations are coupled, since the functional H depends on the total electron density.

As indicated by the linear-response TDDFT calculations, the lowest energy state in the alizarin−TiO_2 system is dominated by a single electronic transition between the orbitals that match the HOMO and the LUMO of free alizarin.[33] This fact justifies two useful approximations: First, the TDDFT calculations employ the PW91 exchange-correlation functional[68] from the family of adiabatic generalized gradient approximation (AGGA) functionals. By using this approximation we assume that the time dependence of the DFT kernel is due to the time dependence of the electron density, which is smooth and driven by the TD external potential of the nuclei. More sophisticated frequency-dependent DFT kernels are in principle more accurate in describing density changes resulting from electronic excitations and constitute an active area of research.[97,98] Since a transition between a pair of single electron wave functions changes the density of the large alizarin−TiO_2 system by a relatively small amount, frequency-dependent effects are small, and the use of an adiabatic kernel is justified. Second, the ET dynamics occurs solely as a result of evolution of the orbital populated by the photoexcitation (Figure 3). This orbital is close in energy to and interacts with the CB of TiO_2. However, on the ultrafast time scale of the injection, the photoexcited orbital does not couple to either the HOMO or the valence band (VB) because of the energy separation (Figure 1). Similarly, the HOMO is not repopulated from the VB. Since the VB orbitals are localized on the semiconductor, their evolution does not contribute to the ET. Only the time dependence of the photoexcited orbital is needed to characterize the ET from alizarin to TiO_2.

The single electron orbitals in TDDFT (eq 2) are expressed in the basis of adiabatic KS orbitals $\phi_k(\mathbf{r}, \mathbf{R}(t))$ that are obtained by a time-independent DFT calculation for the current atomic positions. The adiabatic representation of the photoexcited (PE) orbital

$$\psi_{PE}(\mathbf{r}, t) = \sum_k c_k(t)\phi_k(\mathbf{r}, \mathbf{R}(t)) \quad (3)$$

is inserted into the TD KS eq 2 to obtain the equation for the expansion coefficients:

$$i\hbar\frac{\partial}{\partial t}c_j(t) = \sum_k c_k(t)(\epsilon_k\delta_{jk} + d_{jk}) \quad (4)$$

where ϵ_k is the energy of the adiabatic orbital k, and d_{jk} is the NA coupling between orbitals j and k. The latter is produced by atomic motions that determine the parametric dependence of the adiabatic KS orbitals on time. The NA coupling is calculated numerically by the overlap of orbitals j and k at sequential time steps:[99]

$$d_{jk} = -i\hbar\langle\phi_j|\nabla_{\mathbf{R}}|\phi_k\rangle\cdot\frac{d\mathbf{R}}{dt} = -i\hbar\left\langle\phi_j\left|\frac{\partial}{\partial t}\right|\phi_k\right\rangle \approx -\frac{i\hbar}{2\Delta t}(\langle\phi_j(t)|\phi_k(t+\Delta t)\rangle - \langle\phi_j(t+\Delta t)|\phi_k(t)\rangle) \quad (5)$$

The electronic propagation is performed by the second order differencing scheme[100]

$$c_j(t+\Delta t) = c_j(t-\Delta t) - \frac{2i}{\hbar}\Delta t\sum_k c_k(t)(\epsilon_k\delta_{jk} + d_{jk}) \quad (6)$$

with a 10^{-3} fs time step.

The extent of ET is determined by the fraction of the photoexcited electron that leaves the dye. The portion of the excited electron that remains on the dye is determined by integrating the electron density of the photoexcited state over the region of the simulation cell occupied by the dye:

$$\int_{dye}\rho_{PE}(\mathbf{r}, t)\,d\mathbf{r} = \int_{dye}|\psi_{PE}(\mathbf{r}, t)|^2\,d\mathbf{r} = \sum_{i,j}c_i^*(t)c_j(t)\int_{dye}\phi_i^*(\mathbf{r}, \mathbf{R}(t))\phi_j(\mathbf{r}, \mathbf{R}(t))\,d\mathbf{r} \quad (7)$$

The adiabatic and NA contributions to ET are found by taking the time derivative:

$$\frac{d\int_{dye}\rho_{PE}(\mathbf{r}, t)\,d\mathbf{r}}{dt} = \sum_{i,j}\left\{\frac{d(c_i^*c_j)}{dt}\int_{dye}\phi_i^*\phi_j\,d\mathbf{r} + c_i^*c_j\frac{d\int_{dye}\phi_i^*\phi_j\,d\mathbf{r}}{dt}\right\} \quad (8)$$

The first term corresponds to changes in the occupations of the adiabatic states and represents NA ET. The second term corresponds to changes in the electron density distribution of the adiabatic states and represents adiabatic ET.

Results and Discussion

The ultrafast ET in the alizarin−TiO_2 system is driven by nuclear dynamics and occurs from the photoexcited dye state that is partially delocalized onto the semiconductor. The inhomogeneity in the initial conditions for the ET is determined by the distribution of atomic coordinates at the temperature of the experiment and affects both the degree of the photoexcited-state delocalization and the relative energies of the molecular and surface states. Adiabatic and NA electron injection mechanisms compete on the time scale of the transfer. These factors produce a rich picture of the ET dynamics and are analyzed in detail below.

Donor and Acceptor States. The electron densities of the donor and acceptor states are shown in Figure 5. The states are typical for ET events that originate in donor states with a small amount of delocalization onto TiO_2, which is always the case with photoexcitation below the semiconductor CB and oc-

(97) Onida, G.; Reining, L.; Rubio, A. *Rev. Mod. Phys.* **2002**, *74*, 601.
(98) Botti, S.; Sottile, F.; Vast, N.; Olevano, V.; Reining, L.; Weissker, H.; Rubio, A.; Onida, G.; Sole, R. D.; Godby, R. W. *Phys. Rev. B* **2004**, *69*, 155112.
(99) Hammes-Schiffer, S.; Tully, J. C. *J. Chem. Phys.* **1994**, *101*, 4657.
(100) Leforestier, C.; Bisseling, R. H.; Cerjan, C.; Feit, M. D.; Friesner, R.; Guldberg, A.; Hammerich, A.; Jolicard, G.; Karrlein, W.; Meyer, H. D.; Lipkin, N.; Roncero, O.; Kosloff, R. *J. Comput. Phys.* **1991**, *94*, 59.

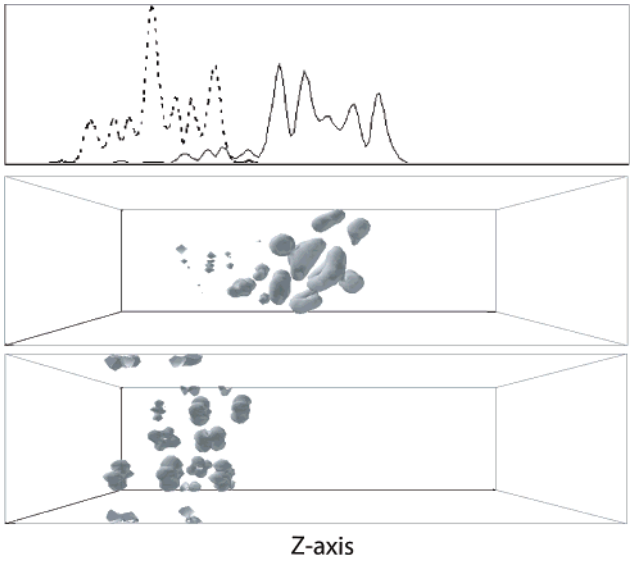

Figure 5. Densities of electron donor and acceptor states. The top panel shows the integrated charge density along the *z* axis, and the bottom two panels show the state densities in a three-dimensional view. The majority of the electron density of the acceptor state is in the first three of five Ti layers. The second and fourth Ti layers appear as two peaks in the top panel because of the alternating orientation of the d-orbitals that maximize their overlap.

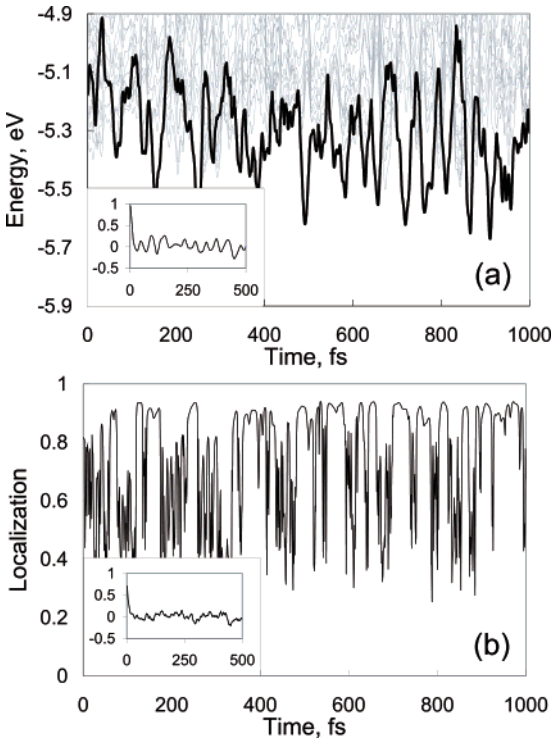

Figure 6. (a) Evolution of the photoexcited state (thick line) and CB state (thin lines) energies. The photoexcited-state energy fluctuates by about 0.15 eV as a result of atomic motions. This is small relative to the 2.5 eV excitation energy, but it moves the dye state into and out of the TiO_2 CB. Insert: The autocorrelation function of the photoexcited state energy indicates a weakly damped oscillation. (b) Evolution of the photoexcited-state localization on the chromophore fragment. Insert: The autocorrelation function of the photoexcited-state localization has a shorter memory than that for the energy, insert in part a.

casionally for photoexcitation deeper in the CB band. Photoexcitation into regions of high CB density mixes the alizarin and TiO_2 orbitals, such that the donor and acceptor states appear as linear combinations of the states shown in Figure 5. The top panel shows donor (solid) and acceptor (dashed) charge density projected onto the direction perpendicular to the surface. The bottom two panels depict the spatial densities of these states in the simulation cell. The donor is a π-state that spans all three rings of the chromophore with only minimal density extending onto the TiO_2 surface, primarily the Ti atom chemically attached to alizarin. The donor state seen in the extended surface calculation matches well with the LUMO of alizarin bound to Ti^{4+} in solution (Figure 3). The acceptor state is entirely in the TiO_2 slab, with no density on the chromophore fragment. It is made up of Ti d-orbitals that are found primarily within the first three Ti layers. The orientation of the d-orbitals alternates between the layers to maximize their overlap. This alternation can be detected in the projected image in the top panel, where the acceptor electron density appears as single peaks in the odd surface layers and doublet peaks in the even layers. Figure 5 indicates that the primary photodriven ET event occurs from a chromophore state with a small amount of density on the semiconductor surface into a localized surface state.

Nuclear Dynamics. Nuclear dynamics have a 2-fold influence on the ultrafast electron injection process. On one hand, in the ground state, thermal fluctuations of the atoms create an ensemble of systems with slightly different geometries and photoexcitation energies. This distribution is responsible for the inhomogeneous broadening of the electronic absorption spectrum (Figure 3). On the other hand, after a photon is absorbed, the nuclear motion along the reaction coordinate gives adiabatic ET (Figure 2). Nuclear motions also promote NA transitions, since the NA coupling is directly proportional to the nuclear velocity (eq 5).

The evolution of the energies of the first photoexcited state and the CB states is presented in Figure 6a. The second photoexcited state is above the energy range of the figure. The thermal fluctuation of the photoexcited state energy has a variance of approximately 0.15 eV. The variance is proportional to the square root of the number of vibrational modes that contribute to the change in the electronic energy. A single atomic vibration has a fluctuation on the order of k_BT, which at room temperature equals 0.025 eV. Since $0.15 \approx 0.025\sqrt{40}$, approximately 40 vibrations, or 13 atoms participate in the atomic motions that lead to the energy fluctuation. For reference, the alizarin chromophore contains 18 heavy atoms.

The inhomogeneous broadening of the photoexcited-state energy due to nuclear fluctuations is much smaller than the chromophore excitation energy or the semiconductor band gap; however, it has a profound effect on the position of the donor state relative to the acceptor manifold. The fluctuation of the energy at room temperature is sufficient to move the photoexcited state into and out of the TiO_2 conduction band, generating two ET regimes. Outside of the band the coupling of the chromophore excited state to the semiconductor states is small. Inside the band the density of states (DOS) grows substantially with increasing energy, and the chromophore excited state can therefore interact with a larger number of TiO_2 states.

An ultrafast production of the alizarin cation is also seen in the alizarin/ZrO_2 system, even though the ZrO_2 CB is approximately 1 eV above the dye excited state[20,21] and therefore out of range of the 0.15 eV thermal fluctuation seen in our simulation. In contrast to TiO_2, however, electron injection from the photoexcited alizarin into ZrO_2 is followed by a rapid

electron recombination with alizarin, indicating that the electron is not able to delocalize into the bulk and is injected into surface trap states that are significantly below the edge of the ZrO_2 CB. Such states can be associated with surface defects and are not seen in our simulation, which employs an ideal TiO_2 surface.

The autocorrelation function (ACF) of the photoexcited-state energy

$$C(t) = \frac{\langle E(t)E(0)\rangle}{\langle E^2\rangle} \tag{9}$$

is shown in the insert of Figure 6a. The ACF describes how much the energy at a particular time depends on its value at earlier times. Generally, poorly correlated random motions give ACFs that decrease rapidly from 1 to 0. Changes that are the result of well-correlated periodic vibrations lead to ACFs that oscillate between 1 and −1. The computed ACF of the photoexcited state energy decreases by approximately 75% within 15 fs but then oscillates continuously for the duration of the simulation. We see similar persistent correlations with other systems, including isonicotinic acid on TiO_2[31] and alizarin attached to a single titanium.[101] Although the 1-ps trajectory used to compute the ACF is too short to definitely ascertain the long-time behavior, it is significantly longer than the 15-fs initial decay, providing sufficient sampling for the first few oscillations seen in the ACF of the insert of Figure 6a. This demonstrates that the evolution of the energy of the photoexcited state is not random and is noticeably influenced by its past evolution.

The fluctuation of the dye energy relative to the CB has a strong effect on the localization of the photoexcited state, which is defined as the fraction of the state's electron density that exists on the alizarin fragment, including the bridging oxygen atoms. When the state is below the CB in energy, it is ≥90% on the alizarin. The state is more substantially delocalized onto the semiconductor when it is inside the CB. The evolution of the photoexcited state localization along the 1-ps trajectory is shown in Figure 6b. The extent of the mixing between the chromophore and semiconductor excited states that determines the localization depends on both the spatial overlap and the energy resonance between the states. The photoexcited state can be strongly localized on alizarin even inside the CB, provided that the isoenergetic CB states are in the bulk. The relative energies and spatial overlap of the alizarin and TiO_2 states change throughout the simulation and lead to values of the localization ranging from >90% to <20%. In cases where the localizations are high, the photoexcited state is very similar to the chromophore excited state. In cases where the localizations are low, the photoexcited state is a superposition of the chromophore state with 1−3 surface states.

The ACF of the photoexcited-state localization is shown in the insert of Figure 6b. In contrast to the energy ACF (insert of Figure 6a), the state localization keeps little memory of its past. This result indicates that the localization is sensitive to a wider, more random set of factors than the energy. It is true in general that the wave function, whose spatial extent determines the localization, is less stable than the energy. For instance, knowledge of the wave function to the first order in perturbation theory immediately gives energy to the second order.

The Fourier transforms (FT) of the photoexcited-state energy and localization trajectories are shown in Figure 7a and b. The energy oscillates with frequencies at and below 700 cm^{-1}, corresponding to bending and torsional motions. Small peaks are seen up to 1600 cm^{-1}, characteristic of C−C and C═O stretches. The insert emphasizes, on a larger scale, that vibrations above 1600 cm^{-1} do not contribute to the oscillation of the photoexcited state energy. Both electronic energy and localization are most strongly modulated by slow motions below 500 cm^{-1}, which is quite typical and has been observed with other systems.[102,103]

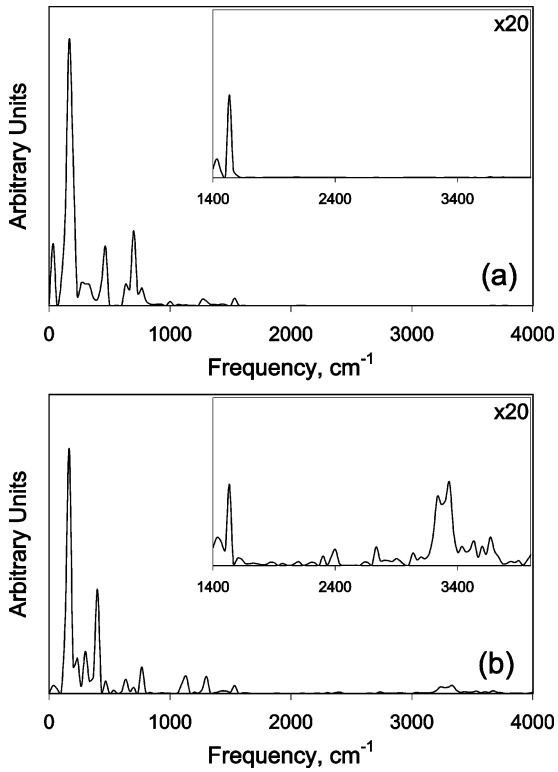

Figure 7. Fourier transforms (FT) of the evolutions of the photoexcited state (a) energy and (b) localization, shown in Figure 6a and b, respectively. Many peaks in the localization FT match the frequencies in the FT of the energy. The additional high-frequency peaks in the localization FT are due to surface hydroxyl groups.

The FT of the photoexcited-state localization (Figure 7b) has similar peaks that correspond to the heavy atom stretches, bends, and torsional motions. As pointed out earlier, the energy resonance is one of the factors that determines the mixing of the chromophore and semiconductor states. Therefore, it can be expected that the motions generating the energy fluctuations also lead to fluctuations in the localization. The difference between the oscillations of the photoexcited-state localization and energy is seen in the high-frequency range, as shown in the insert that covers the same range as the insert in Figure 7a. Unlike the FT of the energy, the localization has several peaks near 3300 cm^{-1}. This spectral region is associated with O−H stretches that are due to the OH groups on the TiO_2 surface. Vibrational modes that involve these groups do not alter the photoexcited-state energy but change both the energies and the spatial extent of the surface states, thereby altering the amount of the semiconductor−chromophore mixing.

(101) Duncan, W. R.; Prezhdo, O. V. *Chem. Phys. Lett.* **2005**, submitted for publication.
(102) Brooksby, C.; Prezhdo, O. V.; Reid, P. J. *J. Chem. Phys.* **2003**, *118*, 4563.
(103) Brooksby, C.; Prezhdo, O. V.; Reid, P. J. *J. Chem. Phys.* **2003**, *119*, 9111.

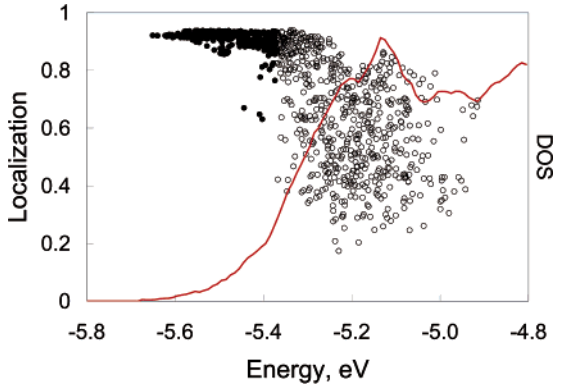

Figure 8. Localization of the photoexcited state on alizarin and the TiO_2 DOS (red line) as functions of energy. Below the CB (filled circles) the photoexcited state is localized on the dye, whereas above the CB (empty circles) the state is delocalized into the semiconductor. The delocalization parallels the increasing TiO_2 DOS. The large spread of the localizations inside the CB is due to fluctuations in the chromophore−semiconductor interaction as discussed in the text.

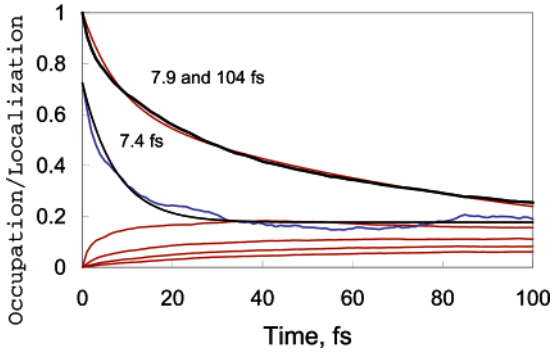

Figure 9. Evolution of the five largest occupations of the adiabatic states, averaged over all NAMD simulations (red lines) and the dye localization of the most occupied state (blue line). The latter decays exponentially with a time constant of 7.4 fs, in agreement with the adiabatic ET time scale (Figure 10). The highest occupation decreases as the electron spreads from the photoexcited state onto other states by the NA mechanism. The electron spreads from surface to bulk after the initial injection, as reflected in the 104-fs component of the double exponential fit.

Photoexcited-State Distribution. Thermal fluctuations of atomic coordinates produce a distribution of the photoexcited-state energies and localizations that creates an inhomogeneous ensemble of initial conditions for the electron injection. The distribution further emphasizes the role of the energy in determining the photoexcited-state localization (Figure 8). Below the CB edge the TiO_2 density of states (DOS) is low, and there is very little mixing between the alizarin excited state and the semiconductor. The localization of the photoexcited state on the alizarin molecule (filled circles) is therefore close to 1. As the energy increases, there are progressively more states to couple to, and the chromophore state is mixed with several semiconductor states. Under these circumstances the localization decreases (empty circles) and significant amounts of ET are produced upon photoexcitation. The large spread in the localization data at higher energies is due to fluctuations in the surface that cause changes in the energies and spatial characteristics of the semiconductor surface states. The DOS shown in the figure is an average over the 1000-fs run. The number of semiconductor states that the chromophore can couple to at a particular energy varies along the run. At a given instance the density of surface states at the alizarin state energy may be substantially greater or less than the average. The surface fluctuations determine how many surface states are available at a given time. Even if the density of acceptor states is the same, the spatial overlap between these states and the chromophore excited state vary substantially between the configurations, depending on the current geometry of the docking region and the orientation of the surface OH groups (cf. FT of localization in Figure 7b). The chromophore excited state can strongly couple to and mix with the semiconductor states. This occurs when there is a nuclear fluctuation that causes surface states to be energetically and spatially close to the molecular state. Despite the spread of the localization data, there is a clear difference between photoexcited states below and above the CB edge. The ET processes in these two cases are noticeably different, as elucidated below.

Adiabatic and Nonadiabatic Electron Dynamics. The evolution of the localizations and occupations of the adiabatic states reflects the mechanism of the ET dynamics. Adiabatic ET occurs by a change in the localization of the occupied state that occurs when the nuclear trajectory passes through a TS (Figure 2). NAET involves a transfer of electron occupation from the photoexcited dye state into semiconductor states, a transfer that is induced continuously by the NA coupling, regardless of a TS. Both effects are simultaneously present in our simulations. Figure 9 shows the time evolution of the five largest occupations of the adiabatic states averaged over all NAMD simulations and the dye localization of the most occupied state. The change in the localization of the most occupied state is directly related to the adiabatic ET. When the data are fit with an exponential, the time constant is 7.4 fs, approximately the same as the time constant for adiabatic ET given below. The highest occupation decreases over the length of the run as the electron spreads over other adiabatic states. This effect cannot be described by a single exponential decay and is fit by a double exponential. The faster 7.9 fs exponential component is 38% in magnitude and roughly corresponds to NA ET, which is slower than 7.9 fs (see below), since not all NA transitions contribute to ET. The longer 104-fs component of the fit describes NA dynamics following the ultrafast electron injection and corresponds to spreading of the electron population from the surface into the bulk.

The dynamics of the electron injection from alizarin to TiO_2 are presented in Figure 10. The ET is determined by the portion of the electron that has left the dye (eq 7). The time scales and relative amounts of adiabatic and NA ET are computed by separating the overall ET evolution into the contributions that are due to changes in the localization and occupation, respectively, according to eq 8. The top panel of Figure 10 shows the total (black), the adiabatic (blue), and the NA (red) ET averaged over all NAMD runs. The total ET is fit by the equation

$$\mathrm{ET}(t) = \mathrm{ET}_f(1 - \exp[-(t + t_0)/\tau]) \qquad (10)$$

where ET_f is the final amount of ET, and τ is the time scale. The fact that the photoexcited state is initially delocalized onto the surface is reflected by the t_0 term of the fit, where t_0 can be interpreted as the time the ET is advanced by the photoexcitation. On average, about 25% of the electron is already inside TiO_2 after the photoexcitation. The adiabatic and NA ET are fit with a similar equation, but without the t_0 term. The time scales for each fit are shown on the figure. For the average over all initial conditions, the adiabatic mechanism dominates the

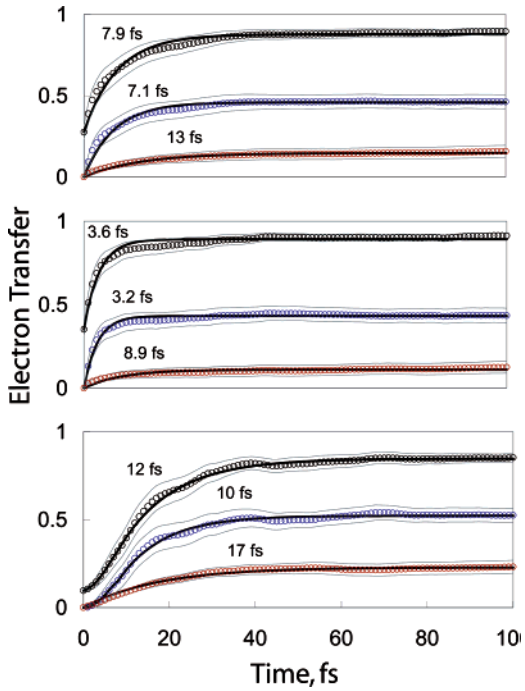

Figure 10. ET dynamics averaged over all initial energies (top), energies above the CB (middle), and energies below the CB (bottom). The black, blue, and red circles (top, middle, and bottom lines in each frame) correspond to the total, adiabatic, and NA ET. The thin gray lines represent 20% of the standard deviation of the ET data. The thick black lines are fits (eq 10) with the time scales shown on the figure.

dynamics and is not only faster but also reaches a much higher value than the NA component. The thin gray lines show 20% of the variance of the data. The variance is quite large, which indicates a large diversity in the individual electron injection events. The variance is initially larger because of the wide range of localizations of the photoexcited state and decreases over time as each NAMD run approaches complete ET. The small oscillations in the total and adiabatic ET data, relative to the fit line, are similar to those observed by Willig and co-workers with perylene[25] and are due to coherent nuclear vibrations.

The ET dynamics averaged over the high and low energy initial conditions corresponding to the photoexcitation above and below the band edge (Figure 8) are distinctly different. The middle panel of the Figure 10 shows the ET dynamics for NAMD runs with the photoexcited state energy above the band gap. The overall shape of the high energy data is similar to that of the top panel. The ET starts from a more delocalized state and proceeds faster. At energies above the CB, the photoexcited state is approximately 35% delocalized into the semiconductor. Both adiabatic and NA transfer components are faster at higher energies. Because the DOS increases with energy (Figure 8), there is a shorter wait until a transition state for adiabatic ET is reached. A larger DOS provides more semiconductor states to couple to, leading to faster NA ET. The electron injection dynamics at high initial energies are even more dominated by the adiabatic mechanism than the dynamics averaged over all initial conditions.

The bottom panel of Figure 10 shows the ET dynamics for NAMD runs from the photoexcited state that is below the conduction band edge (Figure 8). The shape of the overall ET curve and its adiabatic component is markedly different from all other data. The ET is not exponential during the first 8 fs and is best fit by an inverted Gaussian. The Gaussian component of the data reflects the fact that in order for the adiabatic ET to proceed, the donor state must cross with an acceptor state, which can only happen when nuclear motions drive the photoexcited state through the CB edge. Once the dye state has moved into the CB, the ET can be fit with an exponential. The state crossing is not required by NA ET, which behaves exponentially even for the lower energy initial conditions. The 8-fs delay before entering the CB slows down the adiabatic transfer. Because there are fewer semiconductor states with which to couple at low energies, the NA ET is also slower. However, the delay in adiabatic ET and its slower rate once the dye state enters the CB band lead to a larger NA component. The initial states below the CB are well localized on the dye with under 10% of the electron density on the semiconductor. It is quite remarkable that photoexcitation below the CB can lead to fast and efficient electron injection.

Conclusions

A real-time ab initio nonadiabatic molecular dynamics study of the observed 6-fs electron injection from the alizarin chromophore into the TiO_2 surface has provided a detailed mechanistic understanding of the paradoxically ultrafast ET from the molecular donor state into the low-density region of the TiO_2 CB. Most Gratzel cell systems have molecular donors at high-density regions of semiconductor acceptor states.[16−19,36,55,56,64−66] Occasionally, photoexcitation promotes electrons from the chromophore directly into the semiconductor[28,33,53] (Figure 1a). The alizarin−TiO_2 system presents a novel case where the molecular photoexcited state is positioned slightly below the semiconductor CB (Figure 1b). This system architecture presents possibilities for efficient electron injection without the energy loss that is inevitable with injection deep into the CB.

High level ab initio electronic structure analysis of the optical absorption spectrum of alizarin attached to TiO_2 has shown that the photoexcitation proceeds from the molecular HOMO into the system LUMO, which is well-localized on alizarin. The red-shift in the spectrum of free alizarin observed upon binding to TiO_2 occurs as a result of interaction of alizarin LUMO with the CB states. The fact that the LUMO is pushed down in energy indicates that it is located below the CB. The results obtained with a finite size system agree with the corresponding periodic calculations.

Thermal effects included in the periodic calculations are very important in the alizarin−TiO_2 system. A temperature-induced disorder in the atomic coordinates generates an inhomogeneous distribution of photoexcited states, many of which are inside the CB, an effect not seen in the zero temperature calculation. Moreover, even the photoexcited states that are below the edge of the CB at a finite temperature enter the CB band on an 8-fs time scale because of the thermal fluctuation in the atomic positions. This phenomenon, which cannot be seen in a static electronic structure calculation, explains how an efficient ultrafast electron injection becomes possible from molecular states below the CB.

The nonadiabatic molecular dynamics approach developed in our group has allowed us to establish the injection mechanism, resolving the controversy regarding the origin of the ultrafast ET into the low-density CB region. While ultrafast transfer is indeed possible with the nonadiabatic (NA) mechanism and has

been established in other systems,[29] the ET from alizarin to TiO_2 is primarily adiabatic as the result of a strong molecule-semiconductor coupling. The NA component is also observed with the current system and proceeds on an ultrafast, although slower, time scale. The NA mechanism is much weaker in amplitude than the adiabatic ET. The distinction between the adiabatic and NA ET mechanisms is important both from the fundamental viewpoint, since the two represent different theoretical limits and are described by entirely different equations,[57] and from the practical side, since fast adiabatic transfer does not require a high density of acceptor states, has fewer quantum features, and is therefore less sensitive to variation in system properties compared to the NA mechanism. Strong donor−acceptor coupling is required for the adiabatic transfer, which cannot be expected in systems with long donor−acceptor bridges but may still operate in semiconductors such as ZnO and SnO_2 with smaller densities of CB states.

Acknowledgment. The authors thank Dr. Kiril Tsemekhman for fruitful discussions. The research was supported by NSF, CAREER Award CHE-0094012 and PRF, Award 150393. O.V.P. is an Alfred P. Sloan Fellow.

JA042156V